

## Electronic Supplementary Information

### De novo synthesis of hybrid d-f block metal complex salts for electronic charge transport applications

Shreya Mahato,<sup>a</sup> Amit Mondal,<sup>b</sup> Mainak Das,<sup>c</sup> Mayank Joshi,<sup>d</sup> Partha Pratim Ray,<sup>c</sup> Angshuman Roy Choudhury,<sup>d</sup> C. Malla Reddy,<sup>b,\*</sup> and Bhaskar Biswas<sup>a,\*</sup>

<sup>a</sup>*Department of Chemistry, University of North Bengal, Darjeeling 734013, India*

<sup>b</sup>*Department of Chemical Sciences, Indian Institute of Science Education and Research Kolkata, Nadia 741246, India*

<sup>c</sup>*Department of Physics, Jadavpur University, Kolkata 700032, India*

<sup>d</sup>*Department of Chemical Sciences, Indian Institute of Science Education and Research, Mohali, Sector 81, Knowledge City, S. A. S. Nagar, Manauli PO, Mohali, Punjab 140306, India*

---

\*Corresponding author. E-mail: [bhaskarbiswas@nbu.ac.in](mailto:bhaskarbiswas@nbu.ac.in) / [cmr@iiserkol.ac.in](mailto:cmr@iiserkol.ac.in)

## Contents

<b>A. Experimental .....</b>	S3-S8
i. Preparation of the complex salts.....	S3-S4
ii. Physical measurements.....	S4
iii. Crystal structure determination and refinement .....	S5
iv. Device fabrication and characterization to study charge transport properties of the complex salts.....	S5
<b>B. Characterization.....</b>	S5-S8
i.     Spectroscopic and morphological characterization of the complex salts.....	S5-S8
ii.    Electrical characterization of the complex salts.....	S8-S9
<b>C. Figures.....</b>	S10-S19
i. IR spectra.....	S10-S11
ii. UV-Vis spectra.....	S12
iii. Cyclic Voltammogram.....	S13
iv. EPR spectra.....	S14
v. FE-SEM and EDX.....	S15-S16
vi. Crystal engineering perspectives.....	S16-S19
<b>D. Tables.....</b>	S19-S27
i. EPR parameter.....	S19
ii. Bond distances, angles and H- bonding parameters of complex salts 1 & 2.....	S20-S24
iii.    Crystallographic parameters, bond distances and angles of complex salts 3 & 4.....	S25-S27
<b>E. References.....</b>	S27-S28

## A. Experimental

### *Preparation of the complex salts*

#### *(a) Chemicals, solvents and starting materials*

High purity 2,2'-bipyridine (Merck, Germany), 1,10-phenanthroline (Merck, Germany), ammonium ceric nitrate (Aldrich, UK), copper(II) nitrate trihydrate (Merck, India), copper(II) perchlorate hexahydrate (Sigma-Aldrich, USA), copper(II) acetate dihydrate (Merck, India), copper(II) chloride dihydrate (Merck, India), zinc(II) nitrate hexahydrate (Sigma-Aldrich, USA), zinc(II) perchlorate hexahydrate (Sigma-Aldrich, USA) zinc(II) chloride (Sigma-Aldrich, USA) and glacial acetic acid (Merck, India) were purchased from commercial outlets. All the chemicals and solvents were of Analytical grade (A.R. grade) and used as received.

#### *(b) Synthesis of the hybrid complexes salts*

The complex salts (**1-4**) were synthesized by the reaction between metal salts with polypyridyl chelating ligands followed by ceric ammonium nitrate in aqueous acetic acid solution (60/40; v/v). For the preparation of Cu(II)-Ce(IV) complex salts 0.248 g of  $\text{Cu}(\text{NO}_3)_2 \cdot 3\text{H}_2\text{O}$  (1 mmol) in aq. acetic acid was added to 0.312 g of bpy (2 mmol) or 0.360 g of phen (2 mmol) separately followed by the addition of 0.550 g of ceric ammonium nitrate (CAN, 1 mmol) at room temperature. Afterward, the resulting solution was kept on a magnetic stirrer for 30 mins under aerobic atmosphere. The green colour crystalline products for **1** and **2** were separated after 15-20 days and stored in sample vials under moisture-free conditions.

The complex salts **3** and **4** were prepared following the same synthetic approach. Suitable single crystals for the complex salt **3** and **4** were developed under similar reaction conditions and same stoichiometric ratio employing zinc(II) perchlorate hexahydrate with 2,2'-bipyridine and CAN for **3**, and zinc(II) nitrate hexahydrate in combination with 1,10-phenanthroline and CAN for complex salt **4**. The fine microcrystalline compounds were separated after ~15 to 20 days. These were further isolated and dried *in vacuo* over silica gel indicator.

Yield of complex salt **1**: 0.773 g (69.6%). Anal cal. for  $\text{C}_{40}\text{H}_{32}\text{N}_{20}\text{O}_{36}\text{Cu}_2\text{Ce}_2$ : C, 27.05; H, 1.82; N, 15.77; Found: C, 27.01; H, 1.79; N, 15.81. Selected IR bands (KBr pellet,  $\text{cm}^{-1}$ ): 3441( $\nu_{\text{O-H}}$ ), 1642, 1621 ( $\nu_{\text{C=N}}$ ), 1384 ( $\nu_{\text{NO}_3}$ ). UV-Vis ( $\lambda$ , nm,  $10^{-4}$  M, MeCN): 242 (0.93), 298 (0.90), ~730 (0.0016, broad band).

Yield of complex salt **2**: 0.819 g (70.7%). Anal cal. for C<sub>48</sub>H<sub>32</sub>N<sub>16</sub>O<sub>24</sub>Cu<sub>2</sub>Ce: C, 38.85; H, 2.17; N, 15.10; Found: C, 38.74; H, 2.10; N, 15.21. Selected IR bands (KBr pellet, cm<sup>-1</sup>): 3404(v<sub>O-H</sub>), 1634(s), 1608(s) (v<sub>C=N</sub>), 1384(v<sub>NO<sub>3</sub></sub>). UV-Vis ( $\lambda$ , nm, 10<sup>-4</sup> M, MeCN): 269 (1.69), 293(0.63), ~730 (0.0029, broad band).

Yield of complex salt **3**: 0.217 g (73.0%). Anal cal. for C<sub>20</sub>H<sub>16</sub>N<sub>5</sub>O<sub>7</sub>ClZn: C, 44.55; H, 2.99; N, 12.99; Found: C, 25.10; H, 2.20; N, 14.67. Selected IR bands (KBr pellet, cm<sup>-1</sup>): 3402(v<sub>O-H</sub>), 1605(s), 1597(s) (v<sub>C=N</sub>), 1087(v<sub>ClO<sub>4</sub></sub>). UV-Vis ( $\lambda$ , nm, 10<sup>-4</sup> M, MeCN): 237 (1.21), 299(0.61).

Yield of complex salt **4**: 0.241 g (81.1%). Anal cal. for C<sub>48</sub>H<sub>32</sub>N<sub>16</sub>O<sub>24</sub>Zn<sub>2</sub>Ce: C, 38.75; H, 2.17; N, 15.06; Found: C, 38.79; H, 2.73; N, 15.10. Selected IR bands (KBr pellet, cm<sup>-1</sup>): 3423(v<sub>O-H</sub>), 1602, (v<sub>C=N</sub>), 1384 (v<sub>NO<sub>3</sub></sub>). UV-Vis ( $\lambda$ , nm, 10<sup>-4</sup> M, MeCN): 270 (0.98), 290 (0.39).

### **Physical measurements**

Infrared spectra (KBr) were recorded on a FTIR-8400S SHIMADZU spectrophotometer in the range 400–4000 cm<sup>-1</sup>. Ground state UV-Vis absorption was measured with a JASCO V-730 spectrophotometer. Elemental analyses were carried out on a Perkin Elmer 2400 CHN microanalyser. Electron spray ionization (ESI) mass spectra were recorded by a Q-tof-micro quadrupole mass spectrometer. Electrochemical analyses experiments were performed with a conventional three-electrode system. A glassy carbon electrode of surface area 0.07065 cm<sup>2</sup> was used as the working electrode. A platinum wire was used as the counter electrode while Ag/AgCl and saturated KCl were used as the reference electrodes. The temperature during the electrochemical measurements was maintained at 298 K by using the circulating water bath. The electrochemical studies were carried out using *Digi-Ivy*Potentiostat Model DY2312. EPR spectra were recorded at 298 K and 100 K temperature with a BrukerEMM 1843 spectrometer operating at X-band frequency (9.80 GHz). Diphenylpicryl hydroxyl (DPPH) was employed to calibrate the g-values of the complex salts. Low-temperature spectra were recorded using a variable temperature accessory, viz., Eurotherm BVT-2000. EPR spectra of these complex salts in methanol solutions at room temperature were recorded using a flat quartz cell. The morphology and size of the complex salts were assessed by scanning electron microscopy (FE-SEM) images on a microscope in JSM-IT 300HR, JEOL, Japan.

### ***Crystal structure determination and refinement***

Single crystal X-ray diffraction data for the complex salts, **1-4** were collected using a RigakuXtaLABmini (Fixed 2Theta and Distance) diffractometer equipped with Mercury375R (2x2 bin mode) CCD detector. The data were collected with graphite monochromated Mo-K $\alpha$  radiation ( $\lambda=0.71075\text{ \AA}$ ) at 100 K for **1** to **3** and at 293 K for **4** using  $\omega$  scans. The data were reduced using CrysAlisPro 1.171.38.46 suite and the space group determination was done using Olex2. The structures were resolved by direct method and refined by full-matrix least-squares procedures using the SHELXL-97 software package using OLEX<sup>2</sup> suite.<sup>1-3</sup>

### ***Device fabrication and characterization to study charge transport properties of the complex salts***

For the fabrication of metal-semiconductor Schottky device, Indium Tin Oxide (ITO) coated glass substrate was cleaned by acetone, distilled water, and isopropanol repeatedly and sequentially in ultrasonication bath for 20 min. At the same time, a well-dispersed solution of the complex salts (**1-4**) in N,N-dimethylformamide (DMF) medium was prepared followed by spin-coated onto the pre-cleaned ITO coated glass at 600 rpm for 1 min employing SCU 2700 spin coating unit. Repetition of the spin coating step was continued for another 4 times. Thereafter, it was dried in a vacuum. The thickness of the film was measured by the surface profiler and calculated as 1 $\mu\text{m}$ . The aluminum (Al) electrodes were deposited onto the film using the Vacuum Coating Unit (12A4D of HINDHIVAC) under a pressure of 10<sup>-6</sup>Torr. The area of the Al electrodes was maintained as  $7.065\times10^{-6}\text{ m}^2$  with the help of the shadow mask. The measurements of current-voltage of the fabricated device employing the complex salts (**1** and **2**) were carried out by a Keithley 2635B source meter interfaced with PC under the dark condition in the voltage range -1V to +1V at room temperature.

## **B. Characterization**

### ***Spectroscopic and morphological characterization of the Cu(II)-Ce(IV) complex salts***

The synthesized complex salts (**1-4**) were characterized by IR spectra (Fig. S1 & Fig. S2). In the IR spectrum of **1**, moderately strong and sharp peaks at 1642 and 1621 cm<sup>-1</sup> appeared for the presence of coordinated azomethine (-CH=N-) group of bipyridine ligand while a strong peak was observed at 1384 cm<sup>-1</sup> with w-type splitting attributed to the chelation mode of coordination

linkage of nitrate at ceric nitrate ion. A broad peak at  $3441\text{cm}^{-1}$  was also found in the IR spectrum of Cu(II)-Ce(II) complex salt **1** which confirms the presence of intermolecular H-bonding interactions between the oxygen of nitrate with H of bipyridine. The IR spectrum of Cu(II)-Ce(II) complex salt **2** exhibits a broad peak at 3404 and moderately strong peaks at 1634 and  $1608\text{ cm}^{-1}$  which may be attributed to O-H stretching frequency of solvate  $\text{HNO}_3$  and coordinated azomethine group (Fig. S1). The peak at  $1384\text{ cm}^{-1}$  with w-type splitting further indicates the chelation mode of coordination of the nitrate ion to Ce(IV) centre. The IR spectra for the complex salts **3** and **4** exhibit similar stretching frequencies correspond to azomethine and nitrate ( $\sim 1602$  and  $1384\text{ cm}^{-1}$ ) (Fig. S2). The presence of a strong peak at  $1087\text{ cm}^{-1}$  consolidates the existence of  $\text{ClO}_4^-$  ion in **3**. The value of stretching frequencies of O-H,  $\text{NO}_3$ , -C=N- related to their coordination with metal centres are in well agreement with the previously reported values.<sup>4-12</sup>

The electronic spectra were recorded in acetonitrile to understand the solution behaviour of the complex salts (**1-4**) and given in Fig. S3 and Fig. S4. The Cu(II)-Ce(IV) complex salt **1** displayed characteristic bands at 242 and 298 nm while the complex salt **2** exhibited characteristic bands at 269 and 293 nm (Fig. S3). The electronic transitions for both the complex salts in lower than 300 nm appeared for  $\pi\rightarrow\pi^*$  /  $n\rightarrow\pi^*$  electronic transitions of ligand origin<sup>4-12</sup>. Noteworthy, both **1** and **2** exhibited an optical band  $\sim 730$  nm which accounts for the d-d transition of Cu(II) centre for each of the complex salts. The electronic bands for the complex salts **3** and **4** exhibit at 297 and 267 nm respectively. The electronic bands (Fig. S4) are well corroborated with  $\pi\rightarrow\pi^*$  /  $n\rightarrow\pi^*$  transitions of polypyridyl ligands.

The electrochemical nature of the complex salts (**1** and **2**) was analyzed with cyclic voltammetry in an acetonitrile medium. The reduction and oxidation potentials for **1** and **2** which were observed respectively at -800, -300 and +25, + 240 mV (Fig. S5 and S6) at the scan rate of  $20\text{ mVs}^{-1}$  which suggests that the reduction is quite difficult for increasing the electron density significantly on central Cu(II). This is why the reduced species becomes unstable and is oxidized at a positive potential (i.e. + 25 and + 240 mV for **1** and **2** respectively). A plot of the cathodic peak current ( $I_{pc}$ ) with the square root of the scan rate ( $v^{1/2}$ ) for the one-electron reduction shows a linear relationship passing through the origin (Fig. S5b and S6b) for both the complex salts by following equation (2). This plot indicates that the reduction in both the complex salts is purely diffusion-controlled and there is no adsorption at the electrode surface. Using equation (2) and

the plot of  $I_p$  vs.  $(v^{1/2})$  (Fig. S5b and S6b) the diffusion coefficients for the reduction were evaluated as  $1.22 \times 10^{-5}$  and  $2.19 \times 10^{-6} \text{ cm}^2 \text{s}^{-1}$  for Cu(II)-Ce(IV) complex salt (**1**) and Cu(II)-Ce(IV) complex salt (**2**) respectively.

$$I_{pc} = (2.69 \times 10^5) n^{3/2} D_O^{1/2} ACV^{1/2} \quad \dots \dots \dots (2)$$

The cyclic voltammograms of the complex salts at various scan rates showed that with the increase in scan rate the oxidation peak current decreases at completely disappears at a scan rate 100 mVs<sup>-1</sup> and above. This means that the irreversibility of the electrochemical reduction increases with the increase in scan rate, in other word the reversibility of the reduction increases at a slower scan rates. The cyclic voltammetry for the complex salts **3** and **4** were not carried out as the zinc(II) centre and cerium(IV) centre exist in d<sup>10</sup> and f<sup>0</sup> electronic configurations in **3** and **4**.

EPR spectra of the complex salts in  $10^{-3}$  M acetonitrile solutions were also recorded for the complex salts at room and low temperature at X-band frequency. The room temperature EPR spectrum of the complex salts (Figs. S7 and S8) consist of isotropic signal with quartet hyperfine structure exhibiting  $m_I$  dependent line widths typically of copper(II) undergoing tumbling motion (**1**,  $g_{iso}=2.1219$  and  $A_{iso}=72$  G). The EPR spectra of the complex salts in frozen acetonitrile solutions can be described by an axially symmetric spin Hamiltonian,

$$H = g_{\parallel} \beta H_z S_z + g_{\perp} \beta (H_x S_x + H_y S_y) + A_{\parallel} I_z S_z + A_{\perp} (I_x S_x + I_y S_y) \dots \dots (3)$$

where x, y and z refer to the coordinates of the complex, with the symmetry axis in the z direction;  $\beta$  is the Bohr magneton; S= 1/2 is the effective electron spin; I is the nuclear spin (I=3/2 for  $^{63,65}\text{Cu}$  nuclei having 69.2 and 30.8 % of natural abundance); H is the external field; and  $g_{\parallel}$ ,  $g_{\perp}$  and  $A_{\parallel}, A_{\perp}$  are the g values and hyperfine splitting constants respectively, parallel or perpendicular to the symmetry axis. The EPR spectra of frozen complex salts in acetonitrile at 100 K showed an axially symmetric spectrum having quartet hyperfine structure only the parallel components (**1**,  $g_{\parallel} = 2.2776$ ,  $A_{\parallel} = 150$  G,  $g_{\perp} = 2.0521$ ). The typical EPR spectrum of **1** (Fig. S7) showed the presence of nine lines super hyperfine structure ( $^{14}\text{A}_{\text{N}}=15$  G) on the most intense component of the quartet hyperfine structure in the second derivative presentation, confirms a nearly square planar coordination of nitrogen around Cu ions (Fig. S7). The EPR spectrum (Fig. S8) reveals that the structure of complex salt **2** consisted of copper ions situated in distorted six-fold coordination uniquely. The EPR parameter of complex salts in different geometries (distorted square planar and octahedral coordination) agrees well with our heterometallic

complexes (Table S1)<sup>13-17</sup>. The ground state of Ce<sup>4+</sup> ions [Xe]4f<sup>0</sup>5d<sup>0</sup>6s<sup>0</sup>] is diamagnetic and hence EPR silent. The EPR spectra for both the complex salts **3** and **4** were silent and remained EPR inactive.

Field emission scanning electron microscopy (FE-SEM) images and energy dispersive X-ray spectra were also recorded for the newly developed Cu(II)-Ce(IV) and Zn(II)-Ce(IV) complex salts. The FE-SEM image of the complex salt **1** reveals that vertically elongated micro ranged individual particles get agglomerated (Fig. S9). FE-SEM images of the complex salt **2** suggest the existence of irregular but more symmetric micro ranged particles (Fig. S10). The grain size of Cu(II)-Ce(IV) complex salt **2** was found smaller than that of complex salt **1**. Electron dispersive X-ray (EDX) spectral measurement of the complex salts confirmed the similar kind of elemental distribution of Cu, Ce, C, N, and O elements as obtained from the elemental analyses result. The average crystallite size for the complex salts (**1** and **2**) is determined as 677 ( $\pm 3$ ) and 453 ( $\pm 3$ ) nm respectively.

### **Electrical Characterization:**

The Thermionic Emission (TE) theory is adopted to get more insights of the charge transport mechanism in the devices.<sup>18</sup> The current of a diode can be expressed as the following equations according to TE theory.<sup>19</sup>

$$I = I_0 \exp\left(\frac{qV}{\eta kT}\right) \left[ 1 - \exp\left(-\frac{qV}{\eta kT}\right) \right] \quad \dots\dots(S1)$$

Where,

$$I_0 = AA^*T^2 \exp\left(-\frac{q\phi_B}{kT}\right) \quad \dots\dots(S2)$$

$$\phi_B = \frac{kT}{q} \ln\left(\frac{AA^*T^2}{I_0}\right) \quad \dots\dots(S3)$$

Where,  $I_0$  indicates the saturation current,  $q$  represents the electronic charge,  $k$  is the Boltzmann constant,  $T$  is the temperature in Kelvin,  $V$  is the forward bias voltage,  $\eta$  is the ideality factor,  $\phi_B$  is the effective barrier height at zero bias,  $A$  is the diode area ( $7.065 \times 10^{-6}$  m<sup>2</sup>),  $A^*$  is the effective Richardson constant ( $1.20 \times 10^6$  Am<sup>-2</sup>K<sup>-2</sup>). From Cheung, the forward bias I-V characteristics in term of series resistance can be expressed as.<sup>20</sup>

$$I = I_0 \exp\left[\frac{q(V - IR_S)}{\eta kT}\right] \quad \dots\dots(S4)$$

Where, the  $IR_s$  term represents the voltage drop across series resistance of device. In this circumstance, the values of the series resistance can be determined from following functions using equation (7).<sup>21</sup>

According to Cheung's model:

$$\frac{dV}{d\ln(J)} = \left( \frac{\eta kT}{q} \right) + R_S AJ \quad \dots\dots\dots(S5)$$

$$\mathbf{H}(\mathbf{J}) = \mathbf{R}_S \mathbf{A} \mathbf{J} + \boldsymbol{\eta} \phi_B \quad \dots \dots \dots \text{(S6)}$$

and  $H(J)$  can be expressed as:

$$H(J) = V - \left( \frac{\eta kT}{q} \right) \ln \left( \frac{J}{A^* T^2} \right) \quad \dots \dots \dots \quad (S7)$$

### Mott-Gurney SCLC equation

$$I = \frac{9\mu_{eff}\epsilon_0\epsilon_r A}{8} \left( \frac{V^2}{d^3} \right) \quad \dots \dots \dots \quad (S8)$$

Where, I is the current,  $\epsilon_0$  is the permittivity of free space,  $\mu_{\text{eff}}$  is the effective mobility of electron and d is the thickness and  $\epsilon_r$  is the dielectric constant.

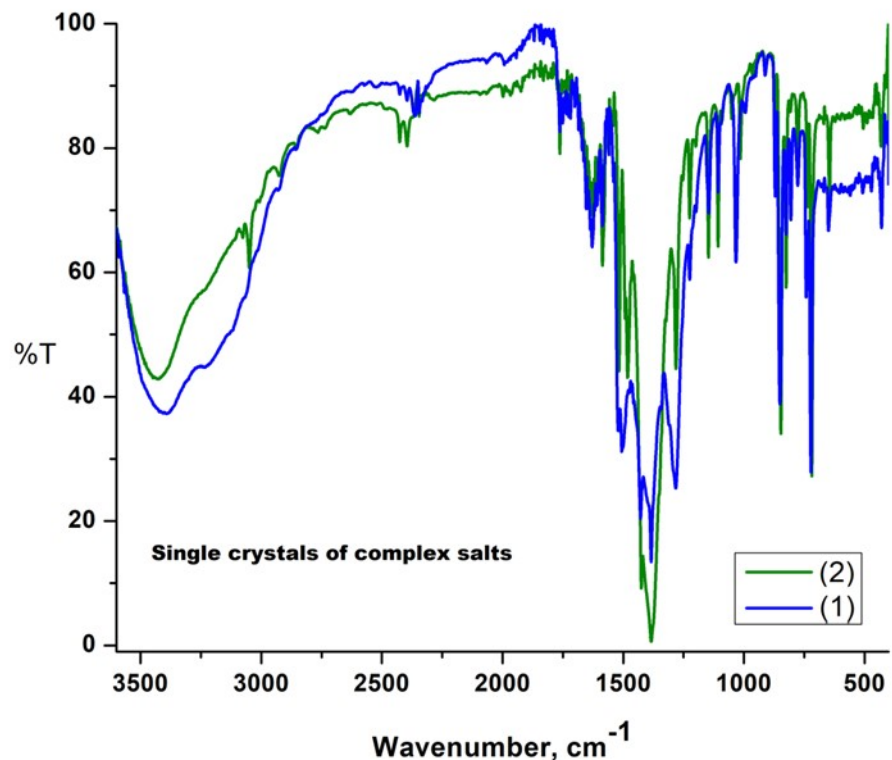


**Fig. S1** IR spectra for the single crystals of the complex salt **1** and **2** (Blue: **1**; Green: **2**)

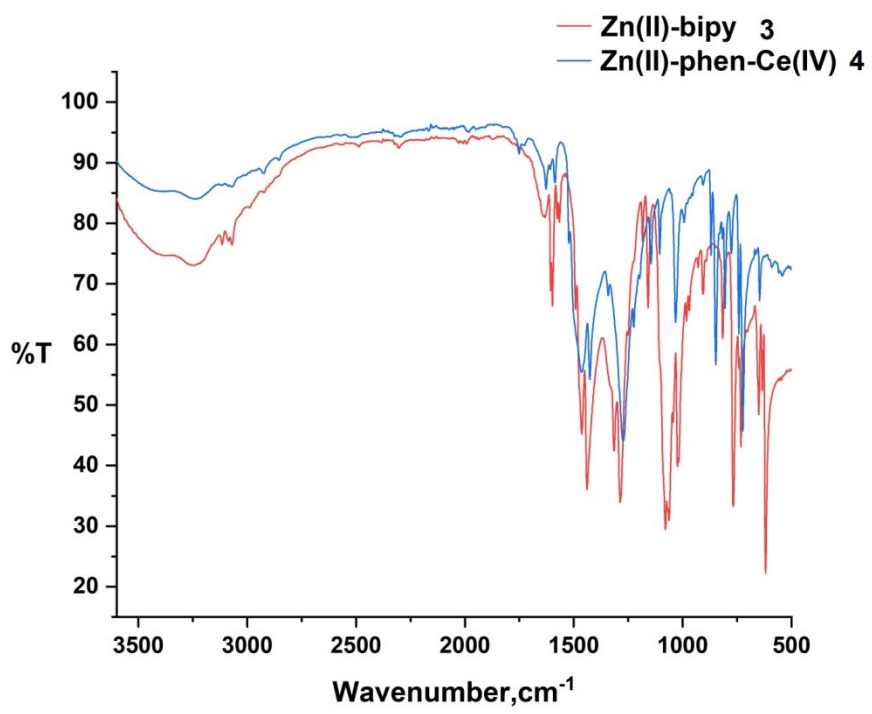


**Fig. S2** IR spectra for the single crystals of the complex salt **3** and **4** (Red: **3**; Blue: **4**)

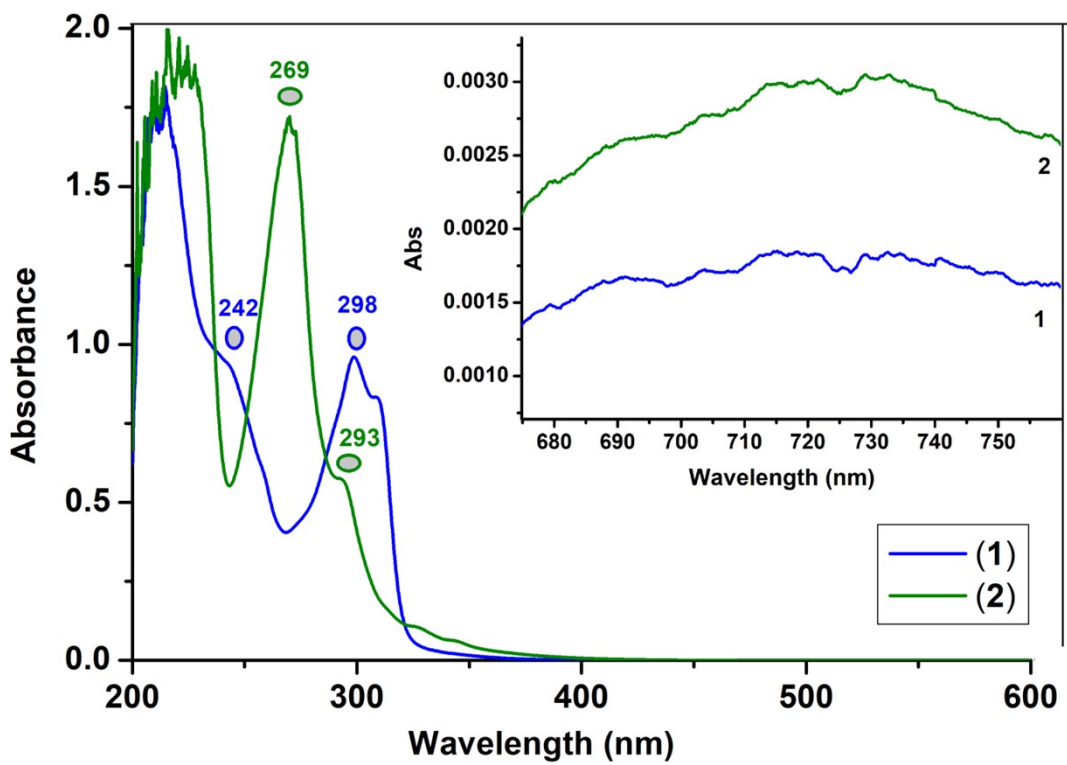


**Fig. S3** UV-Vis spectra of the complex salt **1** and **2** (Blue: **1**; Green: **2**)

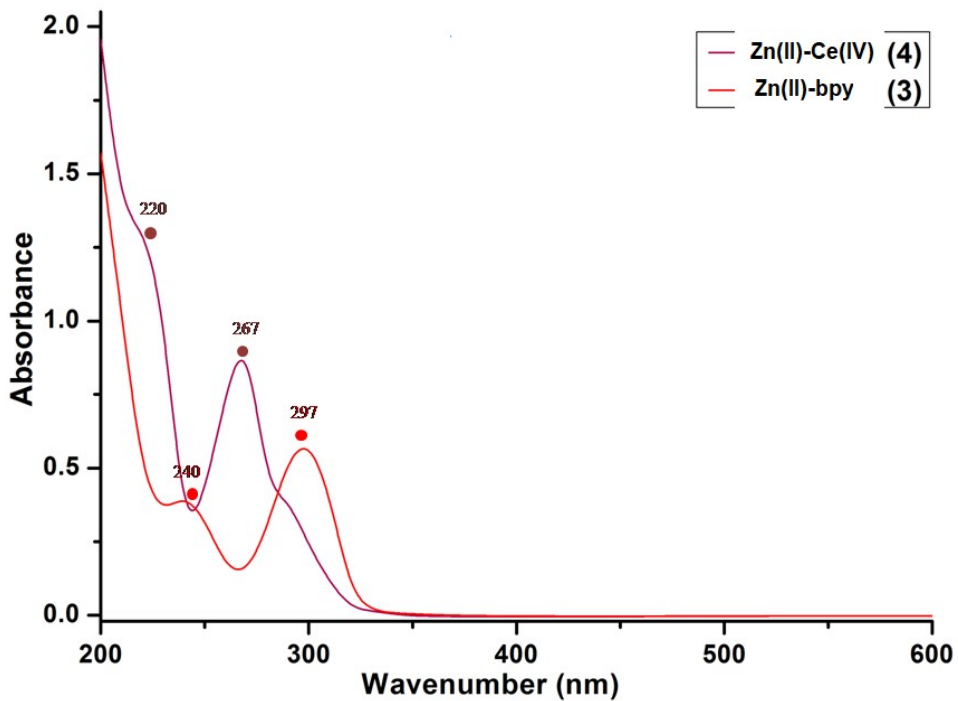


**Fig. S4** UV-Vis spectra of the complex salt **3** and **4** (Red: **3**; Violet: **4**)

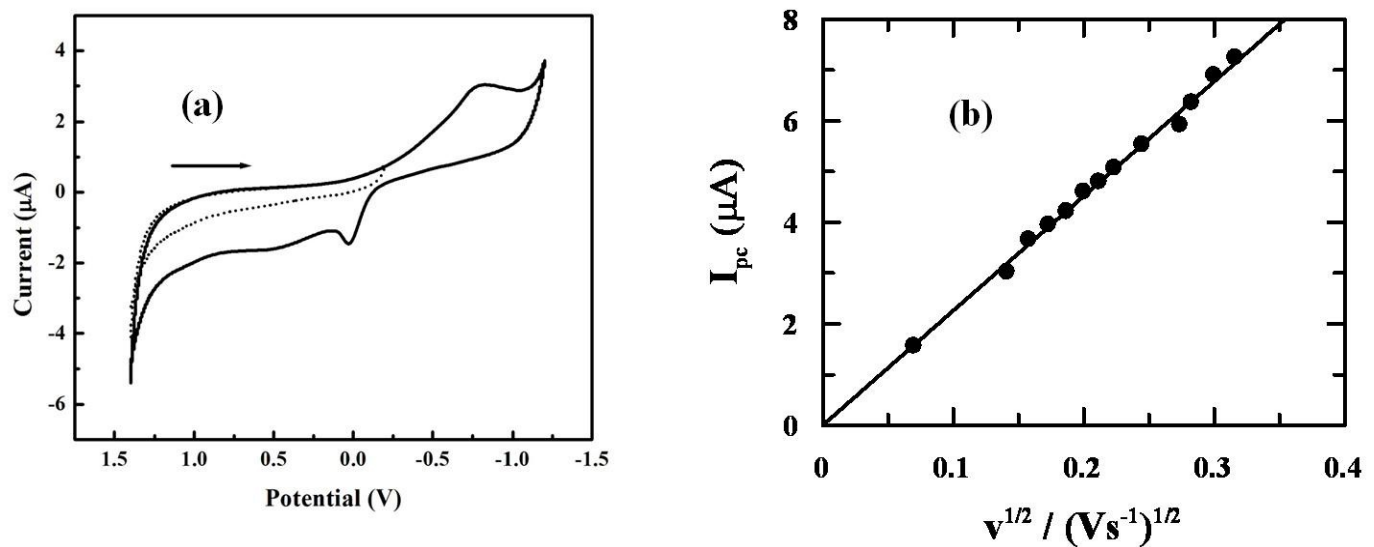


**Fig. S5(a):** Cyclic voltammogram of the complex salt **1** in MeCN. Scan rate: 20  $\text{mVs}^{-1}$ .  $[1] = 10^{-3}$  M,  $[\text{NaF}] = 0.1$  M,  $T = 298.15$  K. **(b):** Plot of cathodic peak current ( $I_{pc}$ ) vs. the square root of the scan rate ( $v^{1/2}$ ) for the reduction of **1**.

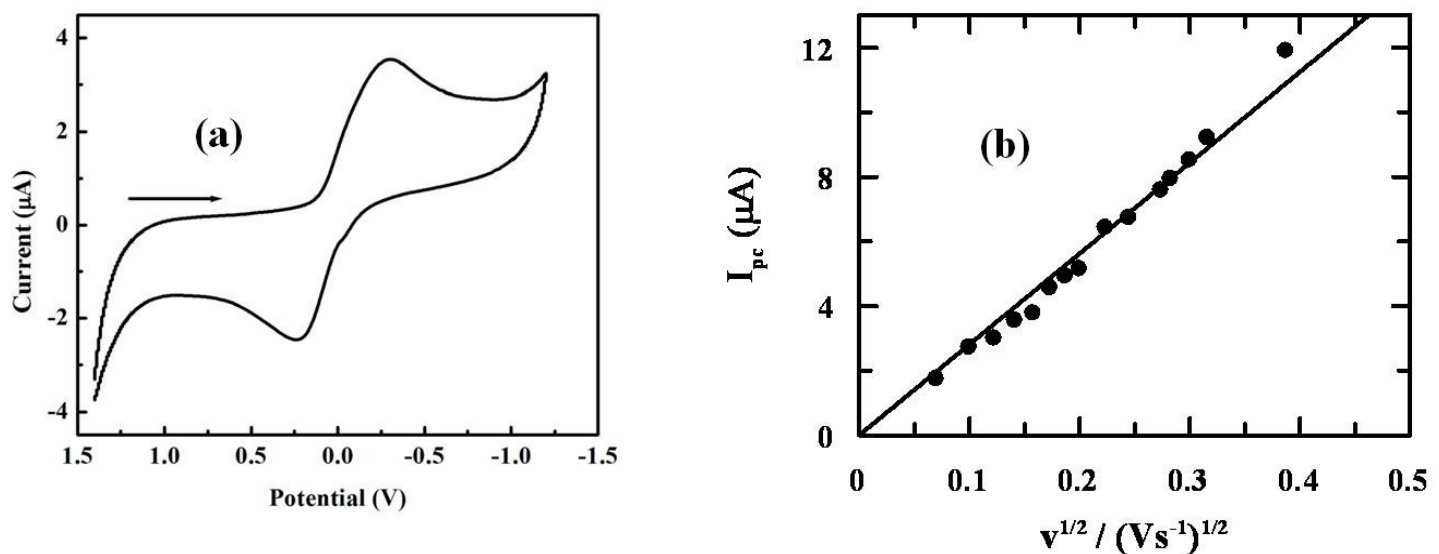


**Fig. S6(a):** Cyclic voltammogram of the complex salt **2** in MeCN. Scan rate: 20  $\text{mVs}^{-1}$ .  $[2] = 10^{-3}$  M,  $[\text{NaF}] = 0.1$  M,  $T = 298.15$  K. **(b):** Plot of cathodic peak current ( $I_{pc}$ ) vs. the square root of the scan rate ( $v^{1/2}$ ) for the reduction of **2**.

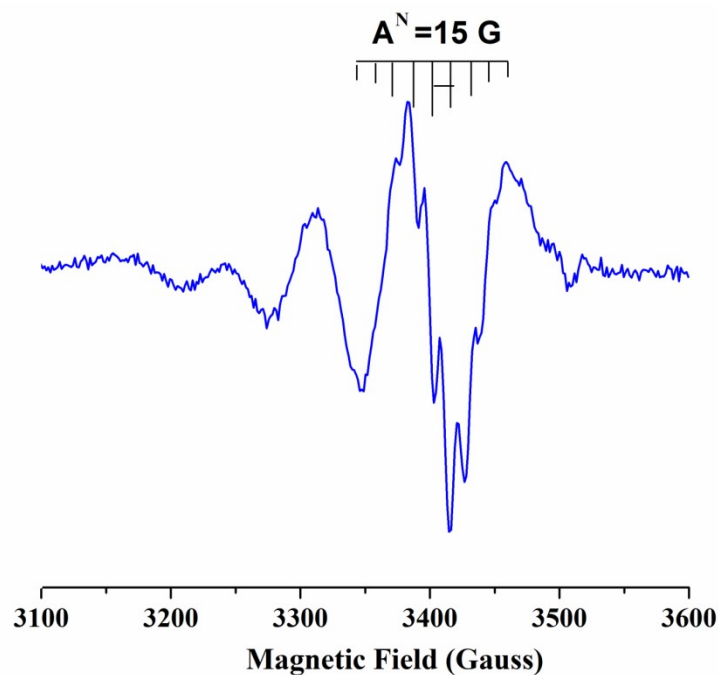


**Fig. S7** EPR spectrum of Cu(II)-Ce(IV) complex salt 1 recorded in second derivative presentation at room temperature. EPR spectrum showed nine line super-hyperfine structures indicating nearly square planar coordination around copper.

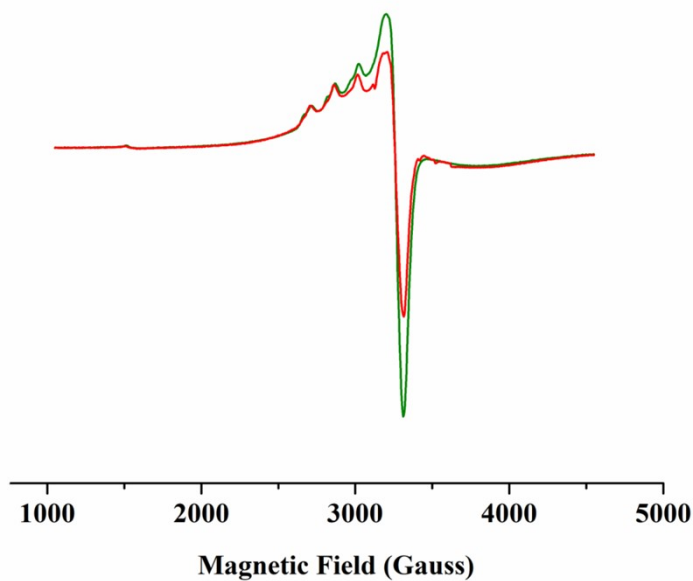


**Fig. S8** EPR spectra of complex salt 2 frozen in acetonitrile recorded at 100 K; (a) black- experimental (a) red-simulated spectrum.

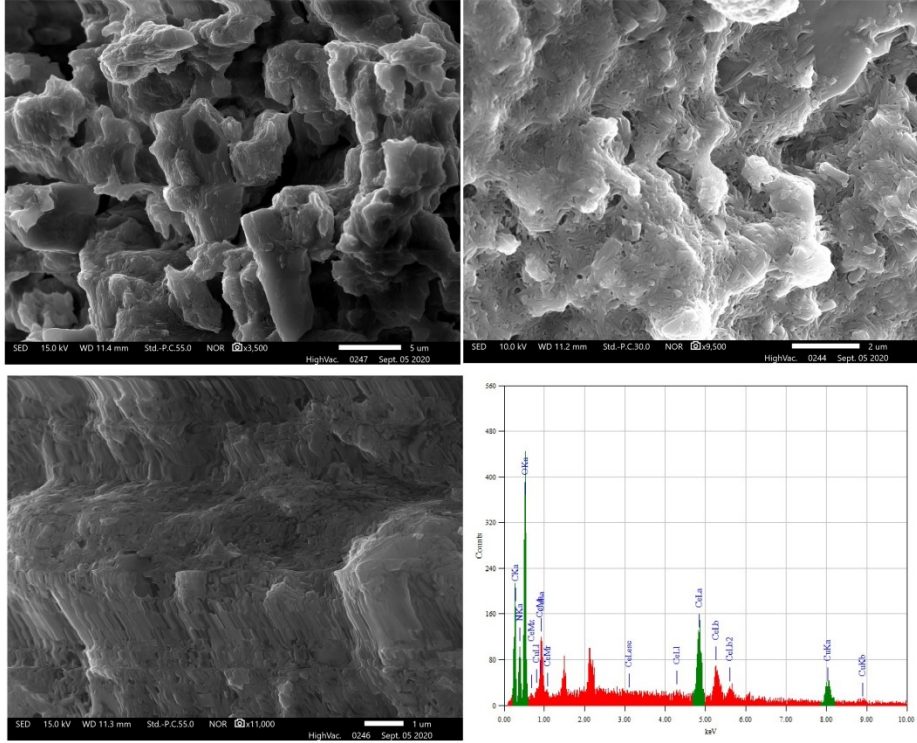


**Fig. S9** FE-SEM micrographs of the Cu(II)-Ce(IV) complex salt (**1**) at different magnification and EDX spectrum of the product

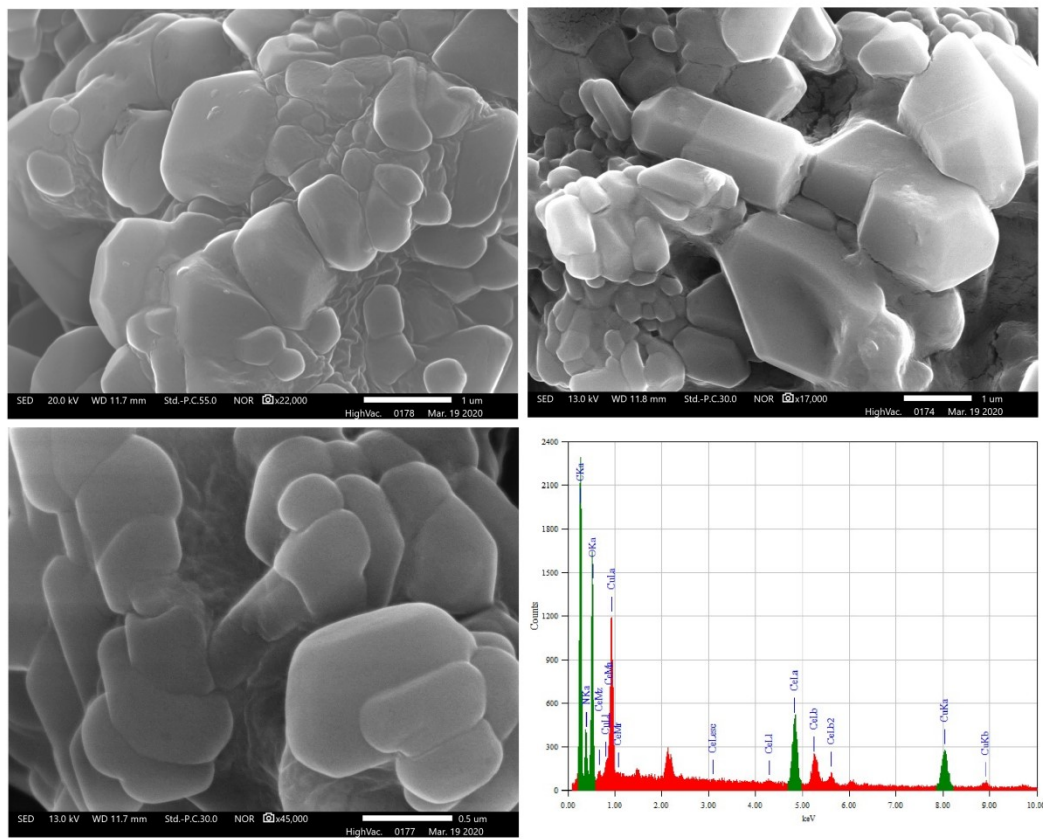


**Fig. S10** FE-SEM micrographs of Cu(II)-Ce(IV)-phen complex salt (**2**) at different magnification and EDX spectrum of the compound

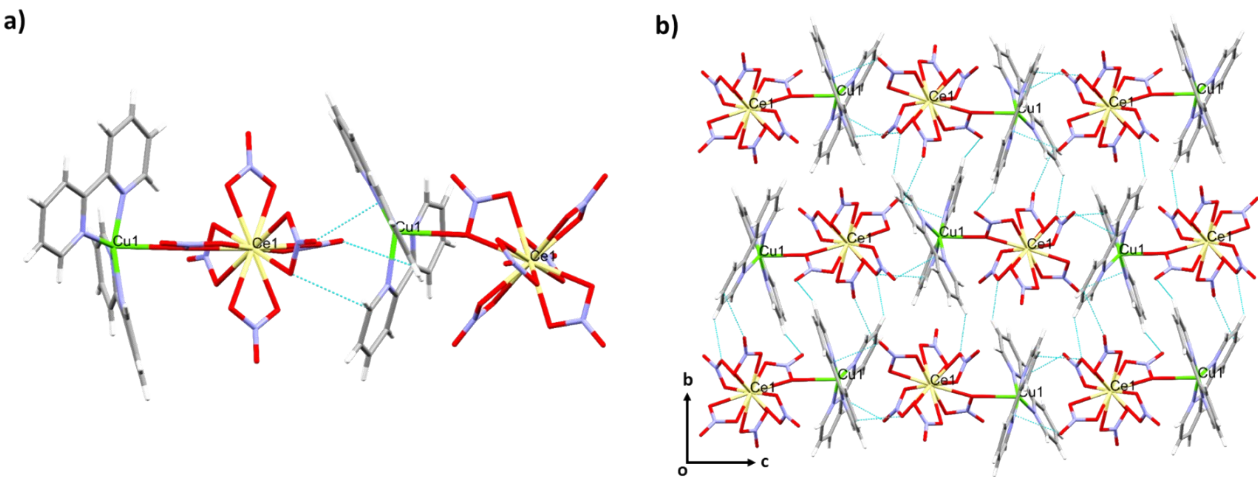


**Fig. S11** Extended crystal structure description of crystal systems a) interaction between Cu<sup>1</sup>(II)-Ce<sup>1</sup>(IV) centres and formation of 1D chain by Cu<sup>1</sup>(II)-Ce<sup>1</sup>(IV) units along the c direction, b) Extension of parallel 1D chains in the b direction in a centrosymmetric manner and thus forming 2D sheet in the bc plane.

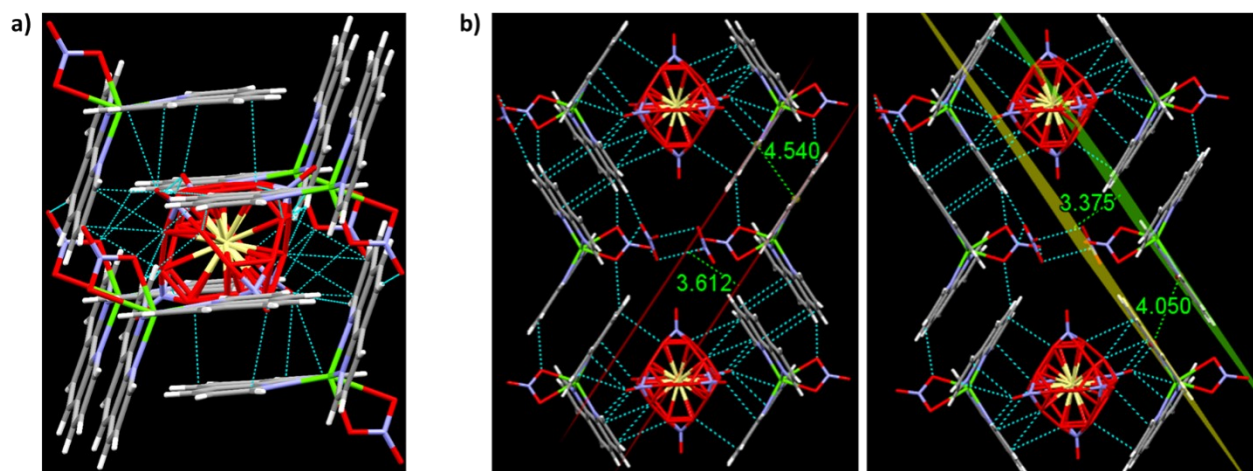


**Fig. S12** Crystal structure description of crystal system 2. a) Capping of the anionic unit by six cationic units, b) Molecular overlay diagram of the cationic units of complexes 2 and 4 involving phenanthroline ligands.

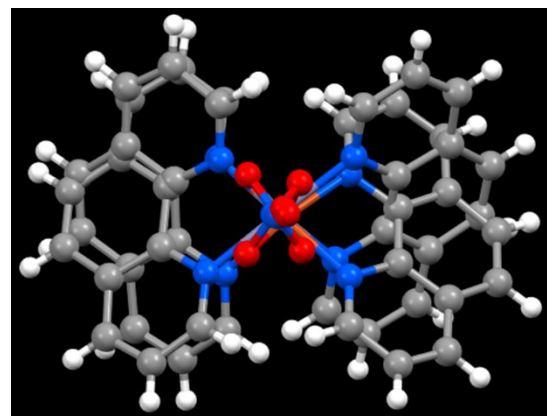


**Fig. S13** Molecular overlay diagram of the cationic units of isostructural complexes 2 and 4 involving phenanthroline ligands.

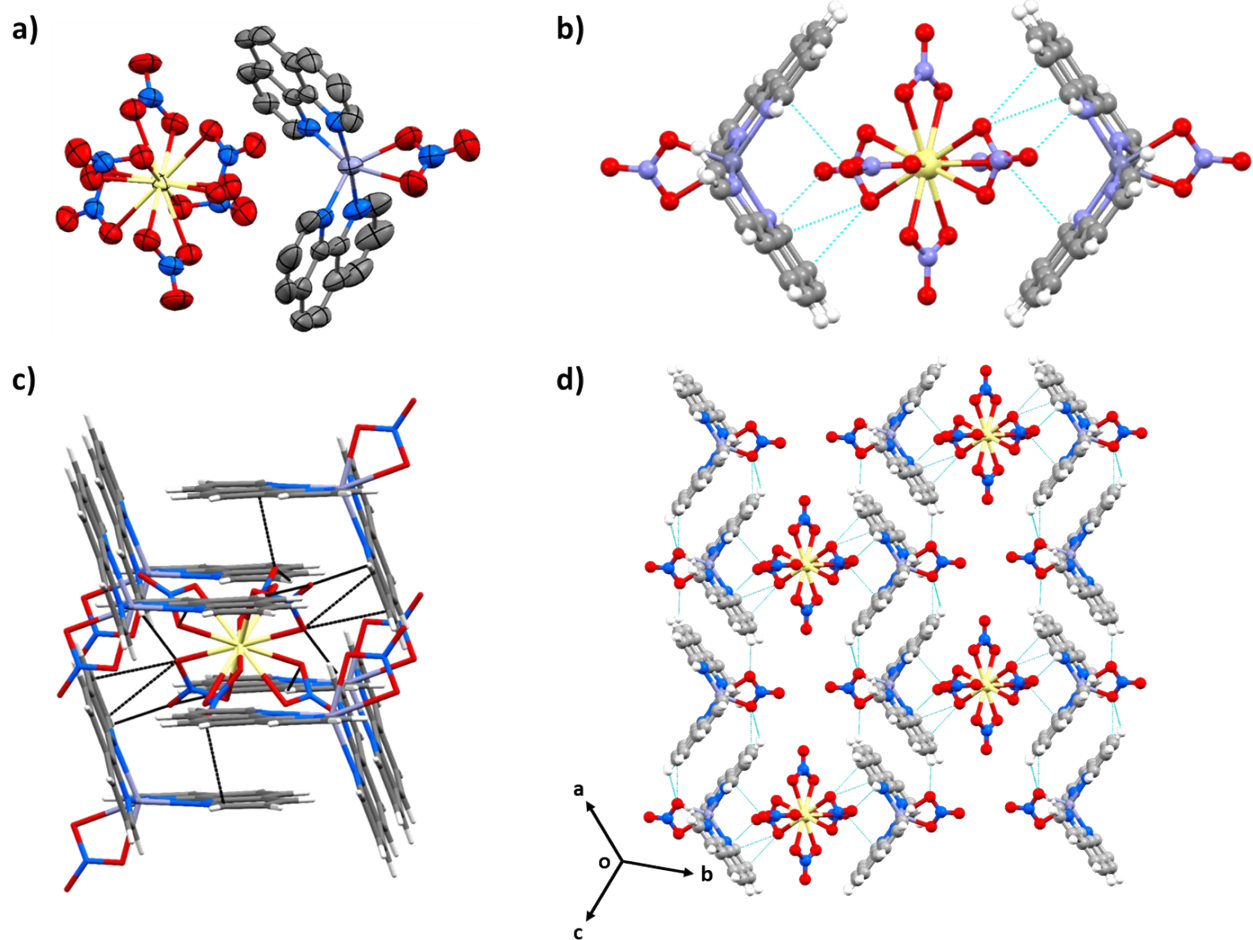


**Fig. S14** Crystal structure description of crystal system 4. a) ORTEP diagram, b) Formation of trimetallic core, c) Capping of the anionic unit by six cationic units, d) extended 3D structure of the trimetallic cores by  $\pi \cdots \pi$  and other interactions.

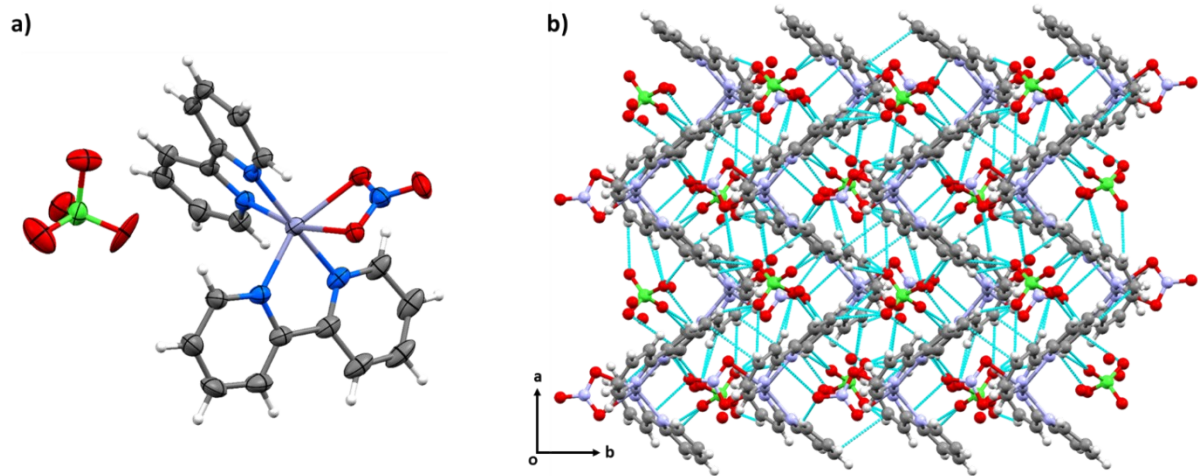


**Fig. S15** Crystal structure description of crystal system 3. a) ORTEP diagram and b) zigzag 3D structure mediated by different O $\cdots\pi$  and C-H $\cdots$ O short contacts.

**Table S1** EPR parameter of copper(II) complexes in different geometries (distorted square planar and octahedral coordination). Hyperfine coupling constant is given in Gauss.

Matrix	$g_{  }$	$g_{\perp}$	$g_{iso}$	$A_{  }$	$A_{\perp}$	$A_{iso}$	Ref
[Cu(NH <sub>3</sub> ) <sub>4</sub> ]; CuN <sub>4</sub>	2.2160	2.0340	2.0947	160	-	-	13
[Cu(NH <sub>3</sub> ) <sub>4</sub> ][PtCl <sub>4</sub> ]; CuN <sub>4</sub>	2.2170	2.0510	2.1063	211	28	89.0	14
[Cu(H <sub>2</sub> O) <sub>6</sub> ]; CuO <sub>6</sub>	2.4090	2.0820	2.1910	144	-	-	15
[CeO <sub>2</sub> :Cu]; CuO <sub>6</sub>	2.2079	2.0403	2.0962	170	27	75.7	16
[Y zeolite:Cu]; CuO <sub>6</sub>	2.330	2.0660	2.1540	160	--	--	17
Complex salt 1; CuN <sub>4</sub>	2.2112	2.0544	2.1067	180	18	72	*
Complex salt 2; CuN <sub>4</sub> O <sub>2</sub>	2.2776	2.0521	2.1273	150	33	72	*

Estimated errors for g value,  $\pm 0.002$ ; for hyperfine splitting,  $\pm 0.5$  G, \* present work, complex salts were frozen in methanol solution.  $A_{\perp}$  value is estimated by using equation  $A_{iso} = (A_{||} + 2A_{\perp})/3$  from room temperature spectra,  $A^N = 15$  G.

**Table S2** Selected bond distances (Å) and angles (°) of the complex salt1

<b>Bond Distance</b>		<b>Bond Distance</b>	
Ce1 -O2	2.501(6)	Ce2 -O20	2.486(6)
Ce1 -O3	2.492(6)	Ce2 -O21	2.476(6)
Ce1 -O5	2.465(7)	Ce2 -O23	2.508(6)
Ce1 -O6	2.456(6)	Ce2 -O24	2.479(6)
Ce1 -O8	2.470(6)	Ce2 -O36	2.531(6)
Ce1 -O9	2.486(6)	Ce2 -O32	2.472(6)
Ce1 -O11	2.475(6)	Ce2 -O33	2.472(6)
Ce1 -O12	2.500(6)	Ce2 -O30	2.496(6)
Ce1 -O14	2.516(6)	Ce2 -O35	2.506(6)
Ce1 -O15	2.500(6)	Cu1 -N2	1.969(7)
Ce1 -O17	2.544(6)	Cu1 -N1	1.994(7)
Ce1 -O18	2.504(6)	Cu1 -N3	1.975(7)
Ce2 -O26	2.490(6)	Cu1 -N4	1.951(7)
Ce2 -O27	2.482(6)	Cu2 -N5	1.967(7)
Ce2 -O29	2.517(6)	Cu2 -N8	1.967(7)
Cu2 -N6	1.969(7)	Cu2 -N7	1.963(6)
<b>Bond Angles</b>			
O2 -Ce1 -O3	50.95(19)	O6 -Ce1 -O8	68.1(2)
O2 -Ce1 -O5	66.7(2)	O6 -Ce1 -O9	69.6(2)
O2 -Ce1 -O6	66.1(2)	O6 -Ce1 -O11	66.41(19)
O2 -Ce1 -O8	66.7(2)	O6 -Ce1 -O12	113.1(2)
O2 -Ce1 -O9	112.99(19)	O6 -Ce1 -O14	129.5(2)
O2 -Ce1 -O11	127.2(2)	O6 -Ce1 -O15	179.5(2)
O2 -Ce1 -O12	177.8(2)	O6 -Ce1 -O17	113.2(2)
O2 -Ce1 -O14	113.2(2)	O6 -Ce1 -O18	113.9(2)
O2 -Ce1 -O15	114.3(2)	O8 -Ce1 -O9	51.2(2)
O2 -Ce1 -O17	113.4(2)	O8 -Ce1 -O11	113.9(2)
O2 -Ce1 -O18	68.86(19)	O8 -Ce1 -O12	115.1(2)
O3 -Ce1 -O5	111.77(19)	O8 -Ce1 -O14	66.69(19)
O3 -Ce1 -O6	112.16(19)	O8 -Ce1 -O15	112.3(2)
O3 -Ce1 -O8	66.26(19)	O8 -Ce1 -O17	178.7(2)
O3 -Ce1 -O9	111.7(2)	O8 -Ce1 -O18	129.0(2)
O3 -Ce1 -O11	178.07(19)	O9 -Ce1 -O11	69.3(2)
O3 -Ce1 -O12	130.66(19)	O9 -Ce1 -O12	68.22(19)
O3 -Ce1 -O14	67.64(19)	O9 -Ce1 -O14	65.1(2)
O3 -Ce1 -O15	68.30(19)	O9 -Ce1 -O15	110.4(2)
O3 -Ce1 -O17	112.68(19)	O9 -Ce1 -O17	129.36(19)
O3 -Ce1 -O18	66.87(19)	O9 -Ce1 -O18	176.4(2)
O5 -Ce1 -O6	51.6(2)	O11 -Ce1 -O12	51.2(2)
O5 -Ce1 -O8	114.1(2)	O11 -Ce1 -O14	114.3(2)
O5 -Ce1 -O9	116.1(2)	O11 -Ce1 -O15	113.12(19)
O5 -Ce1 -O11	66.4(2)	O11 -Ce1 -O17	67.2(2)
O5 -Ce1 -O12	111.1(2)	O11 -Ce1 -O18	112.3(2)
O5 -Ce1 -O14	178.8(2)	O12 -Ce1 -O14	69.0(2)
O5 -Ce1 -O15	128.2(2)	O12 -Ce1 -O15	66.5(2)
O5 -Ce1 -O17	67.0(2)	O12 -Ce1 -O17	64.8(2)
O5 -Ce1 -O18	67.4(2)	O12 -Ce1 -O18	110.04(19)
O14 -Ce1 -O15	50.7(2)	O27 -Ce2 -O35	179.3(2)
O14 -Ce1 -O17	112.25(19)	O27 -Ce2 -O36	130.2(2)
O14 -Ce1 -O18	111.5(2)	O29 -Ce2 -O30	50.66(19)
O15 -Ce1 -O17	66.4(2)	O29 -Ce2 -O32	65.9(2)
O15 -Ce1 -O18	66.1(2)	O29 -Ce2 -O33	113.97(19)
O17 -Ce1 -O18	50.38(19)	O29 -Ce2 -O35	111.4(2)

O20	-Ce2	-O32	114.2(2)	O29	-Ce2	-O36	111.4(2)
O20	-Ce2	-O33	66.79(19)	O30	-Ce2	-O32	67.7(2)
O20	-Ce2	-O35	66.8(2)	O30	-Ce2	-O33	112.5(2)
O20	-Ce2	-O36	67.2(2)	O30	-Ce2	-O35	66.24(19)
O21	-Ce2	-O23	66.8(2)	O30	-Ce2	-O36	65.4(2)
O21	-Ce2	-O24	112.5(2)	O32	-Ce2	-O33	51.9(2)
O21	-Ce2	-O26	66.8(2)	O32	-Ce2	-O35	114.7(2)
O21	-Ce2	-O27	66.41(19)	O32	-Ce2	-O36	69.46(19)
O21	-Ce2	-O29	130.1(2)	O33	-Ce2	-O35	112.4(2)
O21	-Ce2	-O30	179.27(18)	O33	-Ce2	-O36	67.6(2)
O21	-Ce2	-O32	112.5(2)	O35	-Ce2	-O36	50.40(19)
O21	-Ce2	-O33	67.4(2)	O20	-Ce2	-O24	111.59(19)
O21	-Ce2	-O35	113.13(19)	O20	-Ce2	-O26	113.0(2)
O21	-Ce2	-O36	113.9(2)	O20	-Ce2	-O27	112.9(2)
O23	-Ce2	-O24	51.5(2)	O20	-Ce2	-O29	178.2(2)
O23	-Ce2	-O26	68.63(19)	O20	-Ce2	-O30	127.5(2)
O23	-Ce2	-O27	113.7(2)	O20	-Ce2	-O21	51.7(2)
O23	-Ce2	-O29	114.7(2)	O20	-Ce2	-O23	65.3(2)
O23	-Ce2	-O30	113.0(2)	O16	-Cu1	-N2	83.3(2)
O23	-Ce2	-O32	179.3(2)	O16	-Cu1	-O18	45.88(18)
O23	-Ce2	-O33	127.5(2)	O16	-Cu1	-N1	142.2(2)
O23	-Ce2	-O35	65.6(2)	O18	-Cu1	-N1	96.9(2)
O23	-Ce2	-O36	110.53(19)	O18	-Cu1	-N2	79.6(2)
O24	-Ce2	-O26	67.6(2)	O18	-Cu1	-N3	118.2(2)
O24	-Ce2	-O27	113.8(2)	O18	-Cu1	-N4	80.8(2)
O24	-Ce2	-O29	67.63(19)	N1	-Cu1	-N2	83.0(3)
O24	-Ce2	-O30	67.7(2)	O16	-Cu1	-N3	72.9(2)
O24	-Ce2	-O32	129.2(2)	O16	-Cu1	-N4	81.7(2)
O24	-Ce2	-O33	178.16(18)	N2	-Cu1	-N3	104.8(3)
O24	-Ce2	-O35	65.9(2)	N2	-Cu1	-N4	160.3(3)
O24	-Ce2	-O36	111.1(2)	N3	-Cu1	-N4	82.9(3)
O26	-Ce2	-O27	51.0(2)	N1	-Cu1	-N3	144.9(3)
O26	-Ce2	-O29	68.4(2)	N1	-Cu1	-N4	101.3(3)
O26	-Ce2	-O30	113.9(2)	N5	-Cu2	-N7	157.3(3)
O26	-Ce2	-O32	111.38(19)	O36	-Cu2	-N8	109.0(2)
O26	-Ce2	-O33	113.7(2)	N5	-Cu2	-N6	82.7(3)
O26	-Ce2	-O35	128.4(2)	N6	-Cu2	-N8	147.9(3)
O26	-Ce2	-O36	178.7(2)	N7	-Cu2	-N8	82.8(3)
O27	-Ce2	-O29	68.9(2)	O36	-Cu2	-N7	78.5(2)
O27	-Ce2	-O30	114.23(19)	N6	-Cu2	-N7	104.4(3)
O27	-Ce2	-O32	66.0(2)	O36	-Cu2	-N5	78.9(2)
O27	-Ce2	-O33	67.9(2)	N5	-Cu2	-N8	102.9(3)
				O36	-Cu2	-N6	103.1(2)

**Table S3** Geometrical parameters of C-H $\cdots$ O hydrogen bonds ( $\text{\AA}$ ,  $^\circ$ ) involved in the coexistence of individual discrete molecular units in complex salt1. D = donor, A = acceptor ( $\text{\AA}$ ,  $^\circ$ )

D-H $\cdots$ A/(\text{\AA})	d(D-H)	d(H $\cdots$ A)	d(D $\cdots$ A)	$\angle$ D-H $\cdots$ A
C(29) --H(29) ..O(25)	0.95	2.50	3.316(12)	144
C(32) --H(32) ..O(33)	0.95	2.44	3.219(10)	139
C(39) --H(39) ..O(24)	0.95	2.40	3.255(12)	149
C(40) --H(40) ..O(28)	0.95	2.58	3.204(10)	124
C(2) --H(2) ..O(16)	0.95	2.59	3.329(11)	135
C(12) --H(12) ..O(11)	0.95	2.58	3.365(12)	141
C(19) --H(19) ..O(3)	0.95	2.50	3.232(11)	134
C(10) --H(10) ..O(13)	0.95	2.60	3.248	125
C(28) --H(28) ..O(1)	0.95	2.55	3.207(11)	126
C(23) --H(23) ..O(10)	0.95	2.54	3.314(13)	139
C(22) --H(22) ..O(7)	0.95	2.57	3.297(12)	133
C(18) --H(18) ..O(19)	0.95	2.34	3.054(12)	131
C(13) --H(13) ..O(34)	0.95	2.56	3.299(12)	135
C(7) --H(7) ..O(29)	0.95	2.57	3.501(11)	166
C(4) --H(4) ..O(28)	0.95	2.55	3.176(11)	124
C(3) --H(3) ..O(22)	0.95	2.37	3.252(12)	154

**Table S4** Selected bond distances ( $\text{\AA}$ ) and angles ( $^\circ$ ) of complex salt2

Bond Distance		Bond Distance	
Ce1 -O1A	2.495(11)	Ce1 -O4A_a	2.494(13)
Ce1 -O2A	2.513(12)	Ce1 -O5A_a	2.475(11)
Ce1 -O3A	2.466(11)	Ce1 -O6A_a	2.512(12)
Ce1 -O4A	2.494(13)	Ce1 -O3B	2.472(4)
Ce1 -O5A	2.475(11)	Ce1 -O1B	2.510(3)
Ce1 -O6A	2.512(12)	Ce1 -O2B	2.506(3)
Ce1 -O1B_a	2.510(3)	Ce1 -O6B	2.504(4)
Ce1 -O2B_a	2.506(3)	Ce1 -O4B	2.495(4)
Ce1 -O3B_a	2.472(4)	Ce1 -O5B	2.481(3)
Ce1 -O4B_a	2.495(4)	Cu1 -O2	2.546(5)
Ce1 -O5B_a	2.481(3)	Cu1 -O1	2.107(6)
Ce1 -O6B_a	2.504(4)	Cu1 -N1	1.989(4)
Ce1 -O1A_a	2.495(11)	Cu1 -N2	2.089(4)
Ce1 -O2A_a	2.513(12)	Cu1 -N3	2.062(4)
Ce1 -O3A_a	2.466(11)	Cu1 -N4	1.984(5)
Bond Angles		Bond Angles	
O3B -Ce1 -O6B	66.51(11)	O3A_a -Ce1 -O4A	113.3(4)
O1B_a -Ce1 -O3B	67.52(12)	O4A -Ce1 -O4A_a	180.00

O2B_a -Ce1 -O3B	128.86(12)	O4A -Ce1 -O5A_a	67.6(4)
O3B -Ce1 -O3B_a	180.00	O4A -Ce1 -O6A_a	128.8(4)
O3B -Ce1 -O4B_a	113.83(11)	O5A -Ce1 -O6A	112.3(4)
O3B -Ce1 -O5B_a	112.91(11)	O1A_a -Ce1 -O5A	128.8(4)
O3B -Ce1 -O6B_a	113.49(11)	O2A_a -Ce1 -O5A	113.5(4)
O4B -Ce1 -O5B	112.94(13)	O3A_a -Ce1 -O5A	66.6(4)
O4B -Ce1 -O6B	51.03(12)	O4A_a -Ce1 -O5A	67.6(4)
O1B_a -Ce1 -O4B	67.23(12)	O5A -Ce1 -O5A_a	180.00
O2B_a -Ce1 -O4B	68.42(11)	O5A -Ce1 -O6A_a	67.7(4)
O3B_a -Ce1 -O4B	113.83(11)	O1A_a -Ce1 -O6A	113.7(4)
O4B -Ce1 -O4B_a	180.00	O2A_a -Ce1 -O6A	66.9(4)
O4B -Ce1 -O5B_a	67.07(13)	O3A_a -Ce1 -O6A	67.5(4)
O4B -Ce1 -O6B_a	128.97(12)	O4A_a -Ce1 -O6A	128.8(4)
O5B -Ce1 -O6B	67.50(11)	O5A_a -Ce1 -O6A	67.7(4)
O1B_a -Ce1 -O5B	128.73(11)	O6A -Ce1 -O6A_a	180.00
O2B_a -Ce1 -O5B	112.54(11)	O1B_a -Ce1 -O2B_a	113.94(11)
O3B_a -Ce1 -O5B	112.91(11)	O1B_a -Ce1 -O3B_a	112.48(12)
O4B_a -Ce1 -O5B	67.07(13)	O1B_a -Ce1 -O4B_a	112.77(12)
O5B -Ce1 -O5B_a	180.00	O1B_a -Ce1 -O5B_a	51.27(11)
O5B -Ce1 -O6B_a	112.50(11)	O1B_a -Ce1 -O6B_a	66.81(11)
O1B_a -Ce1 -O6B	113.19(11)	O2B_a -Ce1 -O3B_a	51.14(12)
O2B_a -Ce1 -O6B	67.21(12)	O2B_a -Ce1 -O4B_a	111.58(11)
O3B_a -Ce1 -O6B	113.49(11)	O2B_a -Ce1 -O5B_a	67.46(11)
O4B_a -Ce1 -O6B	128.97(12)	O2B_a -Ce1 -O6B_a	112.79(12)
O5B_a -Ce1 -O6B	112.50(11)	O3B_a -Ce1 -O4B_a	66.17(11)
O6B -Ce1 -O6B_a	180.00	O3B_a -Ce1 -O5B_a	67.10(11)
O1A -Ce1 -O2A	67.4(4)	O3B_a -Ce1 -O6B_a	66.51(11)
O1A -Ce1 -O3A	113.0(4)	O4B_a -Ce1 -O5B_a	112.94(13)
O1A -Ce1 -O4A	66.7(4)	O4B_a -Ce1 -O6B_a	51.03(12)
O1A -Ce1 -O5A	51.2(4)	O5B_a -Ce1 -O6B_a	67.50(11)
O1A -Ce1 -O6A	66.3(4)	O1A_a -Ce1 -O2A_a	67.4(4)
O1A -Ce1 -O1A_a	180.00	O1A_a -Ce1 -O3A_a	113.0(4)
O1A -Ce1 -O2A_a	112.7(4)	O1A_a -Ce1 -O4A_a	66.7(4)
O1A -Ce1 -O3A_a	67.0(4)	O1A_a -Ce1 -O5A_a	51.2(4)
O1A -Ce1 -O4A_a	113.4(4)	O1A_a -Ce1 -O6A_a	66.3(4)
O1A -Ce1 -O5A_a	128.8(4)	O2A_a -Ce1 -O3A_a	51.6(4)
O1A -Ce1 -O6A_a	113.7(4)	O2A_a -Ce1 -O4A_a	67.5(4)
O2A -Ce1 -O3A	51.6(4)	O2A_a -Ce1 -O5A_a	66.5(4)
O2A -Ce1 -O4A	67.5(4)	O2A_a -Ce1 -O6A_a	113.1(4)
O2A -Ce1 -O5A	66.5(4)	O3A_a -Ce1 -O4A_a	66.7(4)
O2A -Ce1 -O6A	113.1(4)	O1B -Ce1 -O2B	113.94(11)
O1A_a -Ce1 -O2A	112.7(4)	O1B -Ce1 -O3B	112.48(12)
O2A -Ce1 -O2A_a	180.00	O1B -Ce1 -O4B	112.77(12)
O2A -Ce1 -O3A_a	128.4(4)	O1B -Ce1 -O5B	51.27(11)
O2A -Ce1 -O4A_a	112.6(4)	O1B -Ce1 -O6B	66.81(11)
O2A -Ce1 -O5A_a	113.5(4)	O1B -Ce1 -O1B_a	180.00
O2A -Ce1 -O6A_a	66.9(4)	O1B -Ce1 -O2B_a	66.07(11)
O3A -Ce1 -O4A	66.7(4)	O1B -Ce1 -O3B_a	67.52(12)
O3A -Ce1 -O5A	113.4(4)	O1B -Ce1 -O4B_a	67.23(12)
O3A -Ce1 -O6A	112.5(4)	O1B -Ce1 -O5B_a	128.73(11)
O1A_a -Ce1 -O3A	67.0(4)	O1B -Ce1 -O6B_a	113.19(11)

O2A_a -Ce1 -O3A	128.4(4)	O2B -Ce1 -O3B	51.14(12)
O3A -Ce1 -O3A_a	180.00	O2B -Ce1 -O4B	111.58(11)
O3A -Ce1 -O4A_a	113.3(4)	O2B -Ce1 -O5B	67.46(11)
O3A -Ce1 -O5A_a	66.6(4)	O2B -Ce1 -O6B	112.79(12)
O3A -Ce1 -O6A_a	67.5(4)	O1B_a -Ce1 -O2B	66.07(11)
O4A -Ce1 -O5A	112.4(4)	O2B -Ce1 -O2B_a	180.00
O4A -Ce1 -O6A	51.2(4)	O2B -Ce1 -O3B_a	128.86(12)
O1A_a -Ce1 -O4A	113.4(4)	O2B -Ce1 -O4B_a	68.42(11)
O2A_a -Ce1 -O4A	112.6(4)	O2B -Ce1 -O5B_a	112.54(11)
O2B -Ce1 -O6B_a	67.21(12)	O3B -Ce1 -O4B	66.17(11)
O3B -Ce1 -O5B	67.10(11)	O5A_a -Ce1 -O6A_a	112.3(4)
O3A_a -Ce1 -O6A_a	112.5(4)	O4A_a -Ce1 -O5A_a	112.4(4)
O3A_a -Ce1 -O5A_a	113.4(4)	O4A_a -Ce1 -O6A_a	51.2(4)
O1 -Cu1 -N1	91.2(2)	O1 -Cu1 -N2	100.14(18)
O1 -Cu1 -O2	50.78(19)	O2 -Cu1 -N4	96.2(2)
N1 -Cu1 -N2	82.14(18)	O1 -Cu1 -N3	138.67(18)
O1 -Cu1 -N4	90.7(2)	O2 -Cu1 -N1	86.2(2)
O2 -Cu1 -N2	148.47(17)	O2 -Cu1 -N3	89.63(17)
N3 -Cu1 -N4	81.3(2)	N1 -Cu1 -N3	98.23(18)
N1 -Cu1 -N4	177.5(2)	N2 -Cu1 -N3	120.94(16)
N2 -Cu1 -N4	96.00(18)		

**Table S5** Geometrical parameters of C-H $\cdots$ O hydrogen bonds ( $\text{\AA}$ ,  $^\circ$ ) involved in the coexistence of individual discrete molecular units in complex salt **2**. D = donor, A = acceptor ( $\text{\AA}$ ,  $^\circ$ )

D-H $\cdots$ A/(\text{\AA})	d(D-H)	d(H $\cdots$ A)	d(D $\cdots$ A)	$\angle$ D-H $\cdots$ A
C(1)-H(1) $\cdots$ O2	0.95	2.54	3.121(8)	120
C6 --H6 ..O1	0.95	2.52	3.136(7)	123
C7 --H7 ..O8	0.95	2.54	3.206(8)	127
C15 --H15 ..O13	0.95	2.33	3.227(11)	157
C16 --H16 ..O2	0.95	2.50	3.321(9)	145
C17 --H17 ..O3	0.95	2.57	3.515(9)	174
C19 --H19 ..O3B	0.95	2.33	3.262(8)	168

**Table S6.** Crystallographic structural parameters of the complex salt **3**, Zn(II)-bpy-Ce(IV)

Parameters	Zn-bipy(3)
CCDC No	
Empirical formula	C <sub>16</sub> H <sub>20</sub> N <sub>5</sub> O <sub>7</sub> ClZn
Formula weight	539.21
T (K)	100
Wavelength (Å)	0.71073
Crystal system	Monoclinic
Space group	P2 <sub>1</sub> /n
a (Å)	10.385(4)
b (Å)	12.958(5)
c (Å)	16.648(7)
α (°)	90
β (°)	107.358(16)
γ (°)	90
V (Å <sup>3</sup> )	2138.3(15)
Z	1
ρ (gcm <sup>-3</sup> )	1.677
Absorption coefficient (mm <sup>-1</sup> )	1.329
F(000)	1097
Theta range for data collection	3.0° to 27.5°
Index ranges (h, k, l)	-13: 13 ; -16: 16 ; -21: 21
Reflections collected	21069
Independent reflections	4915
R(int)	0.061
Final R indices [I>2sigma(I)]	R1 = 0.0645, wR2 = 0.1848
Largest diff. peak and hole	1.05,-1.09 e. Å <sup>-3</sup>

**Table S7.** Selected bond distances (Å) and angles (°) of the Zn(II)-bpy complex salt **3**

<b>Bond Distance(Å)</b>			
Zn1 -O1	2.260(3)	Zn1 -O2	2.186(4)
Zn1 -N1	2.129(3)	Zn1 -N2	2.087(4)
Zn1 -N3	2.121(3)	Zn1 -N4	2.080(4)
<b>Bond Angles(°)</b>			
O1 -Zn1 -O2	58.36(12)	O1 -Zn1 -N1	87.12(13)
O1 -Zn1 -N2	95.02(13)	O1 -Zn1 -N3	92.87(11)
O1 -Zn1 -N4	164.62(13)	O2 -Zn1 -N1	88.11(13)
O2 -Zn1 -N2	151.22(14)	O2 -Zn1 -N3	90.62(11)
O2 -Zn1 -N4	108.29(14)	N1 -Zn1 -N2	79.10(13)
N1 -Zn1 -N3	178.52(13)	N1 -Zn1 -N4	100.73(13)
N2 -Zn1 -N3	102.38(12)	N2 -Zn1 -N4	99.42(14)
N3 -Zn1 -N4	78.94(12)		

**Table S8.** Selected bond distances and angles of the complex salt Zn(II)-Phen-Ce(IV)(4)

<b>Bond Distances(Å)</b>			
Ce1-O4*	2.517(3)	Ce1-O5*	2.474(4)
Ce1-O7*	2.503(4)	Ce1-O8*	2.483(3)
Ce1-O10*	2.498(4)	Ce1-O11*	2.505(4)
Ce1-O7	2.503(4)	Ce1-O8	2.483(3)
Ce1-O10	2.498(4)	Ce1-O11	2.505(4)
Ce1-O4	2.517(3)	Ce1-O5	2.474(4)
Zn1-O1	2.119(5)	Zn1-N4	2.098(4)
Zn1-N3	2.128(4)	Zn1-O2	2.392(5)
Zn1-N1	2.091(4)	Zn1 -N2	2.130(5)
<b>Bond Angles(°)</b>			
O7 -Ce1 -O11	113.46(13)	O4* -Ce1 -O5*	50.70(12)
O4* -Ce1 -O7	66.28(12)	O4* -Ce1 -O7*	113.72(12)
O5* -Ce1 -O7	67.52(13)	O4* -Ce1 -O8*	67.64(13)
O7 -Ce1 -O7*	180.00	O4* -Ce1 -O10*	68.44(13)
O7 -Ce1 -O8*	129.25(13)	O4* -Ce1 -O11*	67.25(12)
O7 -Ce1 -O10*	112.47(13)	O5* -Ce1 -O7*	112.48(13)
O7 -Ce1 -O11*	66.54(13)	O5* -Ce1 -O8*	67.45(14)
O8 -Ce1 -O10	67.30(13)	O5* -Ce1 -O10*	113.70(13)
O8 -Ce1 -O11	112.61(13)	O5* -Ce1 -O11*	112.99(11)
O4* -Ce1 -O8	112.36(13)	O7* -Ce1 -O8*	50.75(13)
O5* -Ce1 -O8	112.56(14)	O7* -Ce1 -O10*	67.53(13)
O7* -Ce1 -O8	129.25(13)	O7* -Ce1 -O11*	113.46(13)
O8 -Ce1 -O8*	180.00	O8* -Ce1 -O10*	67.30(13)
O8 -Ce1 -O10*	112.70(13)	O8* -Ce1 -O11*	112.61(13)
O8 -Ce1 -O11*	67.39(13)	O10* -Ce1 -O11*	50.82(14)
O10 -Ce1 -O11	50.82(14)	O4 -Ce1 -O8	67.64(13)
O4* -Ce1 -O10	111.56(13)	O4 -Ce1 -O10	68.44(13)
O5* -Ce1 -O10	66.30(13)	O4 -Ce1 -O11	67.25(12)
O7* -Ce1 -O10	112.47(13)	O4 -Ce1 -O4*	180.00
O8* -Ce1 -O10	112.70(13)	O4 -Ce1 -O5*	129.30(12)

O10 -Ce1 -O10*	180.00	O4 -Ce1 -O7*	66.28(12)
O10 -Ce1 -O11*	129.18(14)	O4 -Ce1 -O8*	112.36(13)
O4* -Ce1 -O11	112.75(12)	O4 -Ce1 -O10*	111.56(13)
O5* -Ce1 -O11	67.01(11)	O4 -Ce1 -O11*	112.75(12)
O7* -Ce1 -O11	66.54(13)	O5 -Ce1 -O7	112.48(13)
O8* -Ce1 -O11	67.39(13)	O5 -Ce1 -O8	67.45(14)
O10* -Ce1 -O11	129.18(14)	O5 -Ce1 -O10	113.70(13)
O11 -Ce1 -O11*	180.00	O5 -Ce1 -O11	112.99(11)
O4* -Ce1 -O5	129.30(12)	O5 -Ce1 -O5*	180.00
O5 -Ce1 -O7*	67.52(13)	O5 -Ce1 -O8*	112.56(14)
O5 -Ce1 -O10*	66.30(13)	O5 -Ce1 -O11*	67.01(11)
O7 -Ce1 -O8	50.75(13)	O7 -Ce1 -O10	67.53(14)
O4 -Ce1 -O7	113.72(12)	O4 -Ce1 -O5	50.70(12)
O1 -Zn1 -N1	142.25(15)	O1 -Zn1 -O2	55.24(17)
O2 -Zn1 -N1	88.65(17)	O1 -Zn1 -N4	103.16(14)
O2 -Zn1 -N3	90.66(17)	O2 -Zn1 -N2	95.15(17)
O1 -Zn1 -N2	92.28(19)	O2 -Zn1 -N4	156.28(16)
N1 -Zn1 -N4	114.17(14)	O1 -Zn1 -N3	92.44(18)
N2 -Zn1 -N4	95.46(14)	N2 -Zn1 -N3	173.95(16)
N1 -Zn1 -N2	79.24(17)	N3 -Zn1 -N4	79.77(14)
N1 -Zn1 -N3	99.23(17)		

## References

- 1 CrysAlisPro 1.171.39.35c, (2017) Rigaku Oxford Diffraction, Rigaku Corporation: Tokyo, Japan.
- 2 G. M. Sheldrick, *Acta Crystallogr. A*, 2015, **71**, 3-8.
- 3 G.M.Sheldrick, *ActaCryst. C*, 2015, **71**, 3-8.
- 4 R.K.Mahato, A.K.Mahanty, S.Paul, V.Gopal,B.Perumalsamy, G.Balakrishnan,; T.Ramasamy,D.Dharumadurai and B.Biswas, *J. Mol. Struct.*, 2020, **1223**, 129264.
- 5 D.Dey, A.Al-Hunaiti, V.Gopal, B.Perumalsamy, G.Balakrishnan, T.Ramasamy,D.Dharumadurai and B.Biswas, *J. Mol. Struct.*, 2020, **1222**, 128919.
- 6 C.K.Pal,S.Mahato, H. R. Yadav, M.Shit, A.R.Choudhury and B.Biswas, *Polyhedron.*, 2019, **174**, 114156.
- 7 D.Dey, M.Patra, A.Al-Hunaiti, H.Yadav, A. Al-mherat, S.Arar, M.Maji, A.R.Choudhury and B.Biswas, *J. Mol. Struct.*, 2019, **1180**, 220-226.
- 8 D.Dey, A.De, H. R. Yadav, P.S.Guin, A.Choudhury, N.Kole and B.Biswas, *ChemistrySelect.*, 2016, **1**, 1910-1916.
- 9 D. Dey, A. De, S. Pal, P. Mitra, A. Ranjani, L. Gayathri,S. Chandraleka, D.Dhanasekaran, M. A. Akbarsha, N. Kole and B. Biswas, *Indian J. Chem. A*,2015,**54A**, 170-178.

- 10 B.Biswas, A.Pal, P.Mitra, F.Tuna, M. Mukherjee and R.Ghosh, *J. Coord. Chem.*, 2012, **65**, 4067-4076.
- 11 (a) D.Dey, H.R.Yadav, A.De, S.Chatterjee, M.Maji, A.R.Choudhury, N.Kole and B.Biswas, *J. Coord. Chem.*, 2014, **68**, 169-180. (b) P.K.Mudi, C.K.Pal and B.Biswas, *Chem. Eur. J.*, 2019, **10**, 125-130.
- 12 D.Dey, S.Das, H.Yadav, A.Ranjani, L.Gyathri, S.Roy, P.Guin, D.Dhanasekaran, A.R.Choudhury, M.A.Akbarsha and B.Biswas, *Polyhedron.*, 2016, **106**, 106-114.
- 13 W.B. Williamson, J.H. Lunsford, *J. Phys. Chem.* 1976, **80**, 2664
- 14 B.J. Hathaway, in: G. Wilkinson, R.D. Gillard, J.A. McCleverty (Eds.), *Comprehensive Coordination Chemistry*, Pergamon Press, 1987, p. 533 (Chapter 53, ref-903).
- 15 V. Bassetti, L.Burlamacchi, G. Martini, J American Chemical Society, 101 (19) (1979) 5471.
- 16 (a) R.Bechara, G. Wrobel, C. F. Aissi, M. Guelton, J. P. Bonnelle and A. Abou-Kais, *Chem. Muter.*, 1990, 2, 518. (b) A. Aboukais, A. Benani, C.F. Aissl, G. Wrobel, M. Guelton, *Chem. Soc. Farad. Trans.* 88 (4) (1992) 615.
- 17 C.C. Chao, J.H. Lunsford, *J. Chem. Phys.* 57 (7) (1972) 2890.
- 18 E. H. Rhoderick and R. H. Williams, *Metal-Semiconductor Contacts*, Clarendon Press, Oxford, 2nd edn, 1988.
- 19 S. M. Sze, *Physics of Semiconductor Devices*, Wiley, New York., 1981.
- 20 S. Sil, R. Jana, A. Biswas, D. Das, A. Dey, J. Datta, D. Sanyal and P. P. Ray, *IEEE Trans. Electron Devices*, 2020, **67**, 2082-2087.
- 21 M. Das, J. Datta, A. Dey, R. Jana, A. Layek, S. Middya and P. P. Ray, *RSC Adv.*, 2015, **5**, 101582-101592